Removal of aqueous toxic Hg(II) by synthesized TiO_2 nanoparticles and TiO_2/montmorillonite

Binlin Dou[a,b]; Valerie Dupont[b,*]; Veiguo Pan[c]; Bingbing Chen[c]

a. Key Laboratory of Ocean Energy Utilization and Energy Conservation of Ministry of Education, Dalian University of Technology 116023, Dalian, China

b, Energy & Resources Research Institute, University of Leeds, Leeds, LS2 9JT, UK

c. School of Energy and Environment Engineering, Shanghai University of Electric Power, Pingliang Rd.2103, 200090 Shanghai, China

Abstract: The adsorption and photocatalytic reduction of toxic Hg(II) in aqueous solutions at different temperatures were investigated with synthesized TiO_2 nanoparticles and TiO_2/montmorillonite. The latter were tested by TGA, BET, TEM and XRD methods. The 9.1nm diameter TiO_2 nanoparticles had a specific surface area exceeding 200 m^2g^{-1}. High purity anatase TiO_2 nanoparticles were produced at 500 °C. TiO_2/montmorillonite was prepared by slurry reactions, resulting in average pore size of 3.10 nm with TiO_2 nanoparticles on the montmorillonite surface. TiO_2/montmorillonite with a 22 wt% TiO_2 load exhibited a specific surface area of 239 m^2g^{-1}. The removal of Hg(II) in aqueous solutions at 25, 35 and 45 °C in darkness and under UV illumination showed that the photocatalytic reduction of Hg(II) increased with increasing temperature, and a decline in adsorption was observed for a raise in temperature from 25 to 45 °C, following the exothermicity of the adsorption process. The adsorption

*, Author to whom correspondence should be addressed. Tel: 44 -113-3432503; Fax: 44 -113-2467310, v.dupont@leeds.ac.uk.

behavior of Hg(II) on the materials were well described by the Langmuir isotherm model, and the adsorption rates were simulated by the Elovich equation. A first-order reaction model was used to simulate the photocatalytic reduction reaction of Hg(II) in aqueous solutions, and a good fit was obtained with the experimental data.

Keywords: TiO_2; montmorillonite; Hg(II), photocatalyst, removal.

1. Introduction

The Hg(II) in industrial wastewaters has received increasing attention as a serious pollutant due to its toxic and bio-accumulative properties [1, 2]. In aquatic systems, Hg(II) are often converted by bacteria to methylmercury, which magnified pose a health risk to humans and wildlife through the aquatic food chain [2]. Thus, it is necessary that effluents from industrial installations be free from its compounds and/or the toxic Hg(II) salts ought to be removed from industrial liquid waste before being discharged into waterways and the biosphere [1]. Several methods have been studied for the removal of Hg(II) in aqueous solutions including activated carbon adsorption, ion-exchange, precipitation and photocatalytic reduction. The adsorption and photocatalytic reduction techniques by TiO_2 materials appear to be most promising because of their high efficiency and simplicity of operation. More importantly, Hg(II) can be removed from the solution by photocatalytic reduction with TiO_2 to elemental mercury which can be safely recovered [3]. Some literatures have illustrated the adsorption and photocatalytic reduction of Hg(II) and Cr(VI) by the TiO_2 powders and the effect of only solution pH has been covered [2-5].

It is well established that morphological and structural parameters strongly affect the adsorption and photocatalytic activity of TiO_2 materials [6-9]. TiO_2 can exist in three crystalline modifications: rutile (tetragonal), anatase (tetragonal), and brookite (orthorhombic). Anatase TiO_2 nanoparticles are the most active allotropic and generally display unique properties, such as quantum size effect, high surface area and short interface migration distance, all of which achieve enhanced photocatalytic performance

[6, 10, 11]. Many methods such as solution phase synthesis [12-15], chemical vapor deposition [16, 17], flame synthesis [18, 19], the alkoxide sol-gel method [20-22], and others [23] have been developed to synthesize anatase TiO_2 nanoparticles. It is well known that nanoparticles have a strong tendency to aggregate in concentrated state, and the aggregation of TiO_2 nanoparticles would lead to the decrease in active surface area of the catalyst, resulting in the decrease in catalytic activity. The anatase phase is also thermodynamically less stable than the rutile phase, and its formation is kinetically favored at lower temperature. Thus, it is not easy to synthesize TiO_2 nanoparticles with high surface area, narrow size distribution and uniform anatase crystalloid [24, 25]. In addition, the synthesis apparatus and product separation should be uncomplicated preferably for low-cost commercial applications [26, 27].

Recently, TiO_2 composites have also been studied by preparing a series of compounds such as microcrystalline TiO_2 pillared clays, mixed Ti/Si, Ti/V oxides, nanocrystals of TiO_2 dispersed in inorganic media [28-34]. Some studies indicated that TiO_2 supported on porous adsorbents is a potential catalyst system for the continuous removal of contaminants from wastewaters [31, 35]. Especially, TiO_2/montmorillonite has been attracting much attention as a new low-cost type of photocatalyst, since its high surface area and superior properties accelerate photocatalytic reactions [32, 35].

The aim of the present investigation is to study the adsorption and photocatalytic reduction of Hg(II) in aqueous solutions by synthesized TiO_2 nanoparticles and TiO_2/montmorillonite. The synthesized materials were characterized by TGA, BET, TEM and XRD. The effects of solution temperatures on the removal of Hg(II) in aqueous solutions were tested. The adsorption equilibrium at different temperatures was studied

by the Langmuir isotherm model. The kinetic models of adsorption and photocatalytic reduction were tested with the experimental data.

2. Experimental

2.1 Materials

2.1.1 Preparation of TiO_2 nanoparticles

We tried to synthesize TiO_2 nanoparticles by applying a controlled acid catalyzed sol-gel method using HNO_3, ethanol and titanium alkoxides, which enables the synthesis of oxide particles with a regulated particle growth through a gel state [24, 25, 35-38]. The sol was prepared using HNO_3, ethanol and titanium alkoxides following the hydrolysis reaction of the Ti precursor in the solution with the temperature of 60-80 °C and the pH of 2-4. The molar ratio of $Ti(OC_4H_9)_4$, ethanol, HNO_3 and deionized water was maintained at 1:20:0.05:3. $Ti(OC_4H_9)_4$ was added dropwise into the mixture solution of ethanol, HNO_3 and deionized water under continuous stirring for 2 h, and a homogeneous pale yellow-green solution was obtained. This was allowed to age at room temperature for 48 h and then dried in an oven at 80 °C for 12 h. It was then calcined in ambient atmosphere at 500 °C for 2 h in a conventional furnace.

2.1.2 Preparation of TiO_2/montmorillonite

Some studies reported the preparation of TiO_2/montmorillonite [28, 32, 33, 38, 39]. Typically, 40 ml of $Ti(OC_4H_9)_4$ were added dropwise into 250 ml of ethanol. The mixture was then added gradually to the HNO_3 solution of 1 mol/L under continuous stirring for 2

h to produce a transparent solution. Subsequently, the pH was adjusted to 2.5 with the addition of 1 M NaOH resulting in a turbid colloid. The pH adjustment was necessary to prevent the destruction of the structure due to reaction with acid. The molar ratio of ethanol, $Ti(OC_4H_9)_4$ and HNO_3 was 12:5:1.6. The montmorillonite used in this study was the sodium-exchanged bentonite. The cation exchange capacity was 83 meq. per 100 g. A mass of 10 g of montmorillonite was saturated with water for half an hour and was firstly modified by cetyltrimethylammonium bromide (CTAB) through an ion-exchange reaction. The basal spacing was further expanded by the intercalation of dodecylamine (DDA) of 20 molar ratio [40]. This was then mixed with a certain amount of TiO_2 sol, stirred for 1 h, followed by a washing-centrifugation procedure to make the supernatant nearly neutral. The mixture was dried for 24 h at 80 °C, calcined at 500 °C for 2 h to remove the organic templates.

2.2 Characterization

The synthesized materials were tested using different techniques. The thermal decomposition behavior of material precursors were examined using a thermo-gravimetric analyzer (model SDT 2960 and thermal analyst 2000, TA instruments). The specific surface areas were determined with the BET method using a Micrometric Acusorb 2100E apparatus. The TiO_2 nanoparticles size was measured by Transmission Electron Microscope (TEM; JEM 4010). The TiO_2 content in the TiO_2/montmorillonite was determined by elemental analysis using X-ray fluorescence method (Rigaku Industrial Corporation, RIX-2000). The X-ray powder diffraction spectra of materials were analyzed using a Shimadzu XRD-6000 powder diffractometer, where a Cu target

Ka-ray (operating at 40 kV and 30 mA) was used as the X-ray source. The particles diameter was also estimated by Scherrer's equation.

2.3 Removal of Hg(II) in aqueous solutions

The experiments of Hg(II) removal were carried out in a cylindrical glass reactor containing 200 ml of $HgCl_2$ (c_0,100 $mg.L^{-1}$) solutions with the temperature control. The pH values of $HgCl_2$ solutions were adjusted to 6.0 by hydrochloric acid. A mass of 2 g of the synthesized materials was used for the tests of Hg^{2+} removal in dark conditions as well as for the tests carried out under UV irradiation by a water-cooled 125 W medium pressure mercury lamp. During the experiments, samples were collected at selected time intervals. In a typical photocatalytic reduction run, the catalyst was suspended in the solution in the dark for 2 hrs by stirring to reach the adsorption equilibrium prior to the photo-reduction experiment under UV irradiation. The Hg(II) concentrations (c, mg/L) in aqueous solutions were analyzed by Cold Vapor Atomic Absorption Spectrometry (CVAAS). In a typical run, the catalyst of TiO_2 nanoparticles was suspended in the solutions and the solutions were continuously stirred for the enhanced diffusion and reaction. The spent materials after experiments were safely kept and treated according to the laboratory regulation.

3. Results and Discussion

3.1 Characterization of TiO_2 nanoparticles and TiO_2/montmorillonite

The TGA results of the precursors of two materials before calcination are shown in Figure 1. The main mass loss values were about 14-17% below 500 °C for TiO_2 nanoparticles and the DTG curve showed decomposition peaks at 350 °C, which may be due to the removal of chemisorbed water and structural hydroxyl groups. The TGA curve of the TiO_2/montmorillonite showed a significant mass loss in the region of 200-450 °C with a maximum at 310 °C from DTG curve, caused by the decomposition of surfactant molecules and the removal of structural hydroxyl groups. The results also indicated the exchange of Na^+ ions with the bulky organic cations CTA^+ in the clay mineral [39-41]. The organic matter degradation in the precursor of TiO_2/montmorillonite is mainly based on C_xH_y decomposition, and water and CO_2 are continuously released, resulting in increase of the basal spacing in layer structure [39-41]. The specific surface area, pore diameter and pore volume for the two materials were determined using nitrogen adsorption/desorption isotherm and multi-point BET analysis, the results of which are shown in Table 1. It can be seen that the specific surface area of the TiO_2 nanoparticles were higher than 200 $m^2\ g^{-1}$. A significant result was that the TiO_2/montmorillonite exhibited the larger specific surface area of 239 $m^2\ g^{-1}$. The synthesized materials were tested and characterized by XRD method. All peaks of XRD patterns of the TiO_2 nanoparticles can be indexed to anatase TiO_2. They were in good agreement with the standard spectrum (JCPDS no.: 21-1272), and no significant peaks of rutile and brookite were observed. The TiO_2 characteristic reflections were observed from the XRD pattern of TiO_2/montmorillonite. Table 2 shows that the TiO_2 content of 22 wt% in the TiO_2/montmorillonite was dramatically higher than that in the purified montmorillonite. The XRD pattern of the pure montmorillonite showed reflections at 2θ = 6.820, 18.921,

28.316. The XRD patterns of the TiO_2/montmorillonite exhibited one diffraction line in the low angle range at 2θ=3.168, which corresponded to a layer spacing expansion [39]. TEM micrographs of the TiO_2 nanoparticles and the TiO_2/montmorillonite (Figure 2) indicated that the TiO_2 nanoparticles obtained by the acid catalyzed sol-gel method were highly dispersed and without great aggregation. Montmorillonite layered silicates exist as platelets of 2-to-1 with a central row of silicate octahedral flanked by two inward-pointing rows of magnesia or alumina. As can be seen from Figure 2(b), the TEM patterns of the TiO_2/montmorillonite showed a cross-linked layer structure, and an aggregated oxide nanoparticles structure is also observed on the surface. Hydrolysis of $Ti(OC_4H_9)_4$ results in formation of either TiO_2 nanoparticle that heterogeneously nucleate on montmorillonite surface to form a shell or some nanoparticles that homogeneously nucleate to form larger nanoparticles. The particles are included in the layer structure and should be less than 3.1 nm, and others of larger sizes were not present in the interlamellar spacing of montmorillonite, and heterogeneously deposited on the external surface [41, 42].

3.2. Formation mechanisms of TiO_2 nanoparticles and TiO_2/montmorillonite

It is interesting to note that the synthesized TiO_2 nanoparticles in this work were uniform anatase, and their size was quite small. It was mentioned earlier that anatase is a thermodynamically less stable phase than rutile. Its formation is typically favored at temperatures of less than 600 °C [30, 43]. This lower temperature could explain the high surface area of the catalysts. The hydrolysis/polycondensation model for the formation of titanium dioxide from the reaction of titanium alkoxides with water in solution phase was

shown in some studies [22, 43-45]. The enhancement effect of solution pH value in the overall hydrolysis reaction is quite straightforward. The dehydroxylation and the dealcoholation are accelerated to increase the overall surface hydrolysis process by acid [45]. During this acid catalyzed sol-gel process, both the formation of sol particles and the gelation process took place, which increased the local pH, resulting in the hydrolyzation of the Ti precursor, and created a dispersion of colloidal particles [22, 43-45]:

$$TiO^{2+} + 2OH^{-} \rightarrow TiO(OH)_2\,(sol) \qquad (R1)$$

Further reaction caused bonds to form between sol particles, resulting in a network of titanium oxyhydroxide gel [45]:

$$TiO(OH)_2(sol) - x\,H_2O \rightarrow TiO_{1+x}(OH)_{2-2x}\,(gel) \qquad (R2)$$

Therefore, the nanoparticles by sol-gel preparation had very small sizes, small pores and single dispersal thus preventing agglomeration.

The possible formation mechanism of mesoporous TiO_2/montmorillonite includes the intercalated quaternary ammonium cations and neutral amines as co-surfactants to direct the interlamellar hydrolysis and condensation polymerization of neutral inorganic precursor [32, 40, 41, 46]. Thus the pore size becomes controllable, and the thermal stability is improved. The montmorillonite has also been proved to be suitable host clay material for the controlled syntheses of catalytically active transition metal particles [32, 35, 46]. Unlike commonly reported microporous pillared structure, a TiO_2 cluster structure in the present study was observed, the purified montmorillonite was firstly modified by cetyltrimethylammonium bromide (CTAB) through an ion-exchange reaction [40, 47]. The basal spacing was further expanded by the intercalation of

dodecylamine (DDA), and then TiO_2 was dispersed and attached in the structure and surface of montmorillonite by hydrolyzing $TiO(OH)_2$ sol using $Ti(OC_4H_9)_4$ as the precursor. Figure 3 shows a schematic of the preparation of TiO_2/montmorillonite. The low hydrolysis reaction will result in the formation of smaller, uniform titanium hydrate and fine TiO_2 particles. The amount of TiO_2 introduced and remaining in the montmorillonite depends on the duration of impregnation and/or the ion exchange procedure. The general schemes for the production of functional nano-structured materials based on delaminated layered silicate particles have also been discussed by some investigators [32, 48]. The other possible mechanisms in forming the TiO_2/montmorillonite included the spaces or pores generated by the 3D co-aggregation of the particles, which was related to the preparation method of nano-structured materials [46].

3.3 Removal of Hg(II) in aqueous solutions

A series of experiments of Hg(II) removal from aqueous solutions by two materials in the dark and under UV illumination were carried out at different temperatures. The experiments in darkness indicated the adsorption of Hg(II) onto the surface of materials. Under the UV illumination, the removal of Hg(II) in aqueous solutions was related to photocatalytic reduction reaction.

3.3.1 Adsorption of Hg(II)

The experimental results of the adsorption of Hg(II) onto the materials at different times are shown in Figure 4. The results showed the adsorption amount of Hg(II)

decreased with increasing temperatures and TiO_2/montmorillonite had a higher adsorption activity compared to TiO_2 nanoparticles. The higher adsorption capacity by TiO_2/montmorillonite could be attributed to its high BET surface area and nanoparticles attached on surface. Hg(II) adsorption isotherm equilibrium on the TiO_2 nanoparticles and TiO_2/montmorillonite at different temperatures are presented in Figure 5. The adsorption behaviors of Hg(II) on the solid materials may be described by the Langmuir adsorption model:

$$q_e = \frac{Q^0 K_L c_e}{1 + K_L c_e} \quad (1)$$

where Q^0 (mg g^{-1}) and K_L (L mg^{-1}) are the Langmuir parameters, related with the maximum capacity of adsorption and with the binding energy of adsorption, respectively; c_e and q_e are the equilibrium liquid-phase concentration of Hg(II) and capacity of solid sample, respectively.

From the corresponding Langmuir parameters, it could be calculated the dimensionless parameter r or separation factor, which is defined as:

$$r = \frac{1}{1 + K_L c_0} \quad (2)$$

According to the calculated r values, $r = 0$ corresponds to irreversible adsorption, $0 < r < 1$ to the favorable equilibrium, $r = 1$ to the linear case and $r > 1$ to unfavorable equilibrium [49, 50].

The Langmuir isotherm adsorption assumes that ions are adsorbed on definite sites that are monoenergetic on the adsorbent surface and each site can accommodate only one molecule or ion. The adsorbed ions cannot migrate across the surface or interact with neighboring molecules. The results by the Langmuir isotherm modeling are shown in

Figure 6. The parameters results by the Langmuir isotherm modeling are shown in Table 3. The adsorbed Hg(II) may be considered to form a tetrahedral complex as $[Hg(OH)_2(H_2O)_2]$ [51]. The Langmuir maximum adsorption capacities (Q^0) decreased with increasing the temperatures, which indicates the exothermic nature of the physical adsorption. The results show that the adsorption isotherm equilibrium of Hg(II) on the TiO_2 nanoparticles and the TiO_2/montmorillonite can be described well by the Langmuir adsorption model.

The kinetic process of adsorption of Hg(II) on solid materials may be described by the Elovich equation, which was established by the work of Zeldowitsch in 1934. In earlier years, the equation has been widely used to describe the kinetics of adsorption of gases onto solids [52]. Recently, the Elovich equation has also been used extensively to describe the adsorption of pollutants from aqueous solutions on solids especially when the adsorption rate decreases with time due to an increased surface coverage of the material [53-57].

$$\frac{dq_t}{dt} = \alpha \exp(-\beta q_t) \qquad (3)$$

where q_t (mg/g) is the amount of Hg(II) adsorption at time t (min), α (mg g^{-1} min^{-1}) is related to the initial adsorption rate, β (g mg^{-1}) is the constant related to the surface coverage of the materials.

To simplify Elovich's equation, some researchers assumed $t >> \frac{1}{\alpha\beta}$ and by applying the boundary conditions of q_t =0 at t = 0 and q_t = q_t at t = t , then Eq. (3) becomes [54-60]:

$$q_t = (\frac{1}{\beta})\ln(\alpha\beta) + (\frac{1}{\beta})\ln(t) \qquad (4)$$

The amount of Hg(II) adsorbed onto the materials, q_t was found by a mass balance relationship:

$$q_t = (c_0 - c)\frac{V}{W} \qquad (5)$$

where V (L) the volume of the solution and W (mg) the mass of the corresponding solid sample.

The equation (6) can be obtained:

$$\frac{c}{c_0} = \varphi \ln(t) + \theta \qquad (6)$$

where $\varphi = -\frac{W}{\beta c_0 V}$; $\theta = 1 - \frac{W}{\beta c_0 V}\ln(\alpha\beta)$

The linear relationship of c/c_0 and $\ln t$ is shown in Figure 7, and the parameters of the Elovich equation including α, β, and correlation coefficients (R) are presented in Table 4. The results show that the Elovich equation can describe this process well. The assumption $t >> \frac{1}{\alpha\beta}$ is justified and the value of α for TiO_2/montmorillonite is larger at a given temperature than that for TiO_2 nanoparticles, which indicates a higher rate of adsorption using TiO_2/montmorillonite.

3.3.2 Photocatalytic reduction of Hg(II)

With the UV illumination, when TiO_2 materials were added into Hg(II) solutions the white TiO_2 turned black with time, indicating Hg was produced. The time profiles of Hg(II) photo-reduction catalyzed by the TiO_2 nanoparticles and TiO_2/montmorillonite

samples are presented in Figure 8. The removal of Hg(II) in aqueous solutions increased with increasing temperatures, and under the 90 min UV illumination at 45 °C, decrease percentages of more than 80% and 90% Hg(II) were achieved with the synthesized TiO_2 nanoparticles and TiO_2/montmorillonite, respectively. Hg(II) concentration in the liquid solutions remained almost constant after 50 min. The dispersed titanium oxides deposited on the surface of montmorillonite or included in layers cavities were used as the photocatalyst showing high efficiency of Hg(II) removal in aqueous solutions. Some studies explained there may due to catalysts having a tetrahedral coordination; resulting in high, characteristic photocatalytic reactivity compared with that the bulk TiO_2 powder catalyst [61]. Considering the influence of the reduction reaction of Hg(II) on catalyst activity, the activity may be high during the initial period. The metallic mercury was then produced and could deposit on the surface of solids to decrease catalyst activity. Moreover, the Hg(II) can become trapped on the surface according to the following reaction [62]:

$$Hg^{2+}(l) + Hg^{0}(s) \leftrightarrow Hg_2^{2+}(s) \qquad \text{(R3)}$$

The overall process of photocatalytic reduction can also be decomposed into several steps including: (a), transfer of the reactants in the fluid phase to the surface; (b), adsorption of the reactants; (c), reaction in the adsorbed phase; (d), desorption of the product; (e), removal of the products from the interface region. The photocatalytic reaction occurs in the adsorbed phase [6]. In the presence of a photocatalyst and UV illumination, Hg(II) can be reduced to Hg by the excited electrons. The photocatalytic reduction of Hg(II) was summarized by the following mechanism [3]:

$$2h\nu + TiO_2 \rightarrow TiO_2 + 2e^{-} + 2h^{+} \qquad \text{(R4)}$$

$Hg^{2+}(aq) \rightarrow Hg^{2+}(ads)$ (R5)

$Hg^{2+}(ads) + 2e^{-} \rightarrow Hg^{0}(ads)$ (R6)

$2H_2O \rightarrow 2H^{+} + 2OH^{-}$ (R7)

$2OH^{-} + 2h^{+} \rightarrow H_2O + 0.5O_2$ (R8)

The net reaction is:

$Hg^{2+}(aq) + H_2O \xrightarrow{hv,TiO_2} Hg^{0}(ads) + 2H^{+} + 0.5O_2$ (R9)

We can illustrate the method of data interpretation with a kinetic model for photocatalytic reaction assuming a first order kinetic model for the reaction rate [3, 34, 63. 64]:

$$c = c_0 \exp(-k_A t) \quad (8)$$

where k_A is the apparent kinetic constant.

The effect of temperature on k_A can also be obtained by changing the temperatures of solutions, and the activation energy for the photocatalytic reduction reaction was further determined by using the following Arrhenius equations:

$$k_A = k_0 \exp(-\frac{E_A}{RT}) \quad (9)$$

where k_0 is the frequency factor.

Plots of the changing concentration of Hg(II) with initial time given by Eq. (8) at different temperatures are shown in Figure 9. The linear relationships between $\ln k_A$ and $1/T$ were well satisfied for the runs, as shown in Figure 9, indicating the kinetic model with the first-order reaction was in excellent agreement with the experimental data. The determined parameters of activation energy and pre-exponential factor are given in Table 5. The apparent activation energies of 25.0 and 22.6 kJ mol^{-1} in Table 5 are in agreement

with the reported value range for Hg(II) photoreduction using photocatalysts, and some studies also indicated the 10-40 kJ mol^{-1} for photocatalysts [6, 65].

4. Conclusions

In this work, we have demonstrated some approaches to the synthesis of TiO_2 nanoparticles and of TiO_2/montmorillonite, and to the removal of toxic Hg(II) in aqueous solutions both by the adsorption and photocatalytic reaction at different temperatures. It was found that the TiO_2 nanoparticles had a narrow size distribution, and the average particles diameter was 9.1 nm. The TiO_2/montmorillonite exhibited the highest specific surface area of 239 m^2 g^{-1} and average pore diameter of 3.10 nm. High purity anatase TiO_2 nanoparticles were produced by heat treatment at 500 °C. The experiments were carried out to test the removal of Hg(II) in aqueous solutions from 25 °C to 45 °C. The results showed that the concentrations of Hg(II) in aqueous solutions increased with increasing temperature within the stated range, indicating a decrease in the adsorption process. TiO_2/montmorillonite exhibiting TiO_2 clusters introduced (and attached) in the montmorillonite is found to behave differently from bulk TiO_2 and exhibit excellent catalytic and adsorption properties. The adsorption of Hg(II) on the materials can be described by the Langmuir isotherm model and the kinetics can be given by the Elovich equation. A kinetic model of a first-order reaction simulated the photocatalytic reduction rate with a good fit, and the activation energies and pre-exponential factors were calculated according to the Arrhenius equation.

Acknowledgement

This work was supported by the Science and Technology Commission of Shanghai Municipality (07DZ12013). The work is supported by the Fundamental Research Funds for the Central Universities (3003-893331)

References

[1] R. Herrero, P. Lodeiro, C. Rey-Castro, T. Vilarino, D. S. Vicente, Removal of inorganic mercury from aqueous solutions by biomass of the marine macroalga Cystoseira baccata, Water Res. 39 (2005) 3199-3210

[2] X. L. Wang, S. O. Pehkonen, A. K. Ray, Photocatalytic reduction of Hg(II) on two commercial TiO_2 catalysts, Electrochim. Acta 49 (2004) 1435-1444.

[3] L. B. Khalil, M. W. Rophael, W. E. Mourad, The removal of the toxic Hg(II) salts from water by photocatalysis, Appl. Catal. B: Environ. 36 (2002) 125-130.

[4] F. Jiang, Z. Zheng, Z. Xu, S. Zheng, Z. Guo, L. Chen, Aqueous Cr(VI) photo-reduction catalyzed by TiO_2 and sulfated TiO_2, J. Hazard. Mater. B134 (2006) 94–103,

[5] F. Zhang, J.O. Nriagu, H. Itoh, Photocatalytic removal and recovery of mercury from water using TiO_2-modified sewage sludge carbon, J. Photochem. Photobiol. A: Chem. 167 (2004) 223-228.

[6] J.M. Herrmann, Heterogeneous photocatalysis: fundamentals and applications to the removal of various types of aqueous pollutants, Catal. Today 53 (1999) 115-129.

[7] D. Igor, A. Denis, J, Zvonko, N. Markus, Nonaqueous synthesis of metal oxide nanoparticles: Short review and doped titanium dioxide as case study for the preparation of transition metal-doped oxide nanoparticles, J. Solid State Chem. 181 (2008) 1571-1581.

[8] V.N.H. Nguyen, R. Amal, D. Beydoun, Effect of formate and methanol on photoreduction/removal of toxic cadmium ions using TiO_2 semiconductor as photocatalyst, Chem. Eng. Sci. 58 (2003) 4429-4439.

[9] F. Thevenet, O. Guaıtella, J.M. Herrmann, A. Rousseau, C. Guillard, Photocatalytic degradation of acetylene over various titanium dioxide-based photocatalysts, Appl. Catal. B: Environ. 61 (2005) 58–68.

[10] C. Sriwong, S. Wongnawa, O. Patarapaiboolchai, Photocatalytic activity of rubber sheet impregnated with TiO_2 particles and its recyclability, Catal. Commun. 9 (2008) 213-218.

[11] M. Saquib, M.A. Tariq, M. Faisal, M. Muneer, Photocatalytic degradation of two selected dye derivatives in aqueous suspensions of titanium dioxide, Desalination 219 (2008) 301-311.

[12] M.C. Hidalgo, M. Aguilar, M. Maicu, J.A. Navıo, G. Colon, Hydrothermal preparation of highly photoactive TiO_2 nanoparticles, Catal. Today 129 (2007) 50–58.

[13] S.W. Oh, S.H. Park, Y.K. Sun, Hydrothermal synthesis of nano-sized anatase TiO_2 powders for lithium secondary anode materials, J. Power Sources 161 (2006) 1314-1318.

[14] F. Sayılkan, S. Erdemoğlu, M. Asiltürk, M. Akarsu, S. Şener, S. Sayılkan, S. Erdemoğlu, E. Arpaç, Photocatalytic performance of pure anatase nanocrystallite TiO_2 synthesized under low temperature hydrothermal conditions, Mater. Res. Bull. 41 (2006) 2276-2285.

[15] S. Yamabi, H. Imai, Synthesis of rutile and anatase films with high surface areas in aqueous solutions containing urea, Thin Solid Films 434(2003) 86-93.

[16] T. Chou, T. Ling, M. Yang, C. Liu, Micro and nano scale metal oxide hollow particles produced by spray precipitation in a liquid–liquid system, Mater. Sci. Eng. A 359 (2006) 24-30.

[17] A.R. Rao, V. Dutta, Low-temperature synthesis of TiO_2 nanoparticles and preparation of TiO_2 thin films by spray deposition, Sol. Energ. Mat. Sol. C. 91 (2007) 1075-1080.

[18] K. Nagaveni, G. Sivalingam, M. Hegde, G. Madras, Photocatalytic Degradation of Organic Compounds over Combustion-Synthesized Nano-TiO_2, Environ. Sci. Technol. 38 (2004) 1600-1604.

[19] T. Sahm, L. Mädler, A. Gurlo, N. Barsan, S.E. Pratsinis, U.Weimar, Flame spray synthesis of tin dioxide nanoparticles for gas sensing, Sensor. Actuat. B: Chem. 98 (2004) 148-153.

[20] M. Crişan, A. Brăileanu, M. Răileanu, M. Zaharescu, D. Crişan, N. Drăgan, M. Anastasescu, A. Ianculescu, I. Niţoi, V.E. Marinescu, S.M. Hodorogea, Sol-gel S-doped TiO_2 materials for environmental protection, J. Non-Cryst. Solid. 354 (2008) 705-711.

[21] R.S. Sonawane, S.G. Hegde, M.K. Dongare, Preparation of titanium(IV) oxide thin film photocatalyst by sol–gel dip coating, Mater. Chem. Phys. 77 (2003) 744-750.

[22] N.B. Shali, S. Sugunan, Influence of calcination ambient and film thickness on the optical and structural properties of sol–gel TiO_2 thin films, Mater. Res. Bull. 42 (2007) 1777-1783.

[23] C. Wu, J. Huang, J. Wen, S. Wen, Y. Shen, M. Yeh, Preparation of TiO_2 nanoparticles by supercritical carbon dioxide, Mater. Lett. 62 (2008) 1923–1926.

[24] P.P. Ahonen, U. Tapper, E.I. Kauppinen, J. Joubert, J. Deschanvres, Aerosol synthesis of Ti–O powders via in-droplet hydrolysis of titanium alkoxide, Mater. Sci. Eng. A 315 (2001) 113-121.

[25] M. Kanna, S. Wongnawa Mixed amorphous and nanocrystalline TiO_2 powders prepared by sol–gel method: Characterization and photocatalytic study, Mater. Chem. Phys. 110 (2008) 166-175.

[26] G. Chen, G. Luo, J. Xu, J. Wang, Membrane dispersion precipitation method to prepare nanopartials, Powder Technol. 139 (2004) 180-185.

[27] S. Mahshid, M. Askari, M. Ghamsari, Synthesis of TiO_2 nanoparticles by hydrolysis and peptization of titanium isopropoxide solution, J. Mater. Process. Tech. 189 (2007) 296–300.

[28] V. Belessi, D. Lambropoulou, I. Konstantinou, A. Katsoulidis, P. Pomonis, D. Petridis, T. Albanis, Structure and photocatalytic performance of TiO_2/clay nanocomposites for the degradation of dimethachlor, Appl. Catal. B: Environ. 73 (2007) 292-299.

[29] X. Ding, T. An, G. Li, S. Zhang, J. Chen, J. Yuan, J. Zhao, H. Chen, G. Sheng, J. Fu, Preparation and characterization of hydrophobic TiO_2 pillared clay: The effect of acid hydrolysis catalyst and doped Pt amount on photocatalytic activity, J. Colloid Interface Sci. 320 (2008) 501-507.

[30] Y. Gao, Y. Masuda, W. Seo, H. Ohta, H. Koumoto, TiO_2 nanoparticles prepared using an aqueous peroxotitanate solution, Ceram. Int. 30 (2004) 1365-1368.

[31] A. Fernández, G. Lassaletta, V.M. Jiménez, A. Justo, A.R. González-Elipe, J.M. Herrmann, H. Tahiri, Y. Ait-Ichou, Preparation and characterization of TiO_2 photocatalysts supported on various rigid supports (glass, quartz and stainless steel). Comparative studies of photocatalytic activity in water purification, Appl. Catal. B: Environ. 7 (1995) 49-63.

[32] R. Kun, K. Mogyorósi, I. Dékány, Synthesis and structural and photocatalytic properties of TiO_2/montmorillonite nanocomposites, Appl. Clay Sci. 32 (2006) 99-110.

[33] K. Shimizu, T. Kaneko, T. Fujishima, T. Kodama, H. Yoshida, Y. Kitayama, Selective oxidation of liquid hydrocarbons over photoirradiated TiO_2 pillared clays, Appl. Catal. A: Gen. 225 (2002) 185-188.

[34] J. Yang, J. Zhang, L. Zhu, S. Chen, Y. Zhang, Y. Tang, Y. Zhua, Y. Li, Synthesis of nano titania particles embedded in mesoporous SBA-15: Characterization and photocatalytic activity, J. Hazard. Mater. B137 (2006) 952–958.

[35] G. Li, X. Zhao, M. Ray, Advanced oxidation of orange II using TiO_2 supported on porous adsorbents: The role of pH, H_2O_2 and O_3, Sep. Purif. Technol. 55 (2007) 91-97.

[36] S. Doeuff, M. Henry, C. Sanchez, J. Livage, Hydrolysis of titanium alkoxides: Modification of the molecular precursor by acetic acid, J Non-Cryst. Solid. 89 (1987) 206-216.

[38] W. Guo, Z. Lin, X. Wang, G. Song, Sonochemical synthesis of nanocrystalline TiO_2 by hydrolysis of titanium alkoxides, Microelectron. Eng. 66 (2003) 95-101.

[39] J. Liu, M. Dong, S. Zuo, Y. Yu, Solvothermal preparation of TiO_2/montmorillonite and photocatalytic activity, Appl. Clay Sci. 43 (2009) 156-159.

[40] L. Yan, J. Wang, H. Yu, Q. Wei, B. Du, X. Shan, Adsorption of benzoic acid by CTAB exchanged montmorillonite, Appl. Clay Sci. 37 (2007) 226-230.

[41] O.S. Ahmed, D.K. Dutt, In situ generation of metal clusters in interlamellar spacing of montmorillonite clay and their thermal behavior, Thermochim. Acta 395 (2002) 209-216.

[42] L. Xiang, X. Zhao, Preparation of montmorillonite/titania nanocomposite and enhanced electrorheological activity, J. Colloid Interface Sci. 296 (2006) 131–140.

[43] T. Sugimoto, X. Zhou, Synthesis of Uniform Anatase TiO_2 Nanoparticles by the Gel–Sol Method: 2. Adsorption of OH^-Ions to $Ti(OH)_4$ Gel and TiO_2 Particles, J. Colloid Interface Sci. 252 (2002) 347-353.

[44] J.T. Banks, T. Yu, H. Yu, Direct Visualization of the Hydrolysis Kinetics of Titanium(IV) Alkoxides on Functionalized Gold Surfaces, J. Phys. Chem. B 106 (2002) 3538-3542.

[45] I. Zuo, C. Nie, X. Gu, Y. Lai, Y. Zong, L. Sun, C. Lin, Fabrication of TiO_2/Au nanorod arrays employing a positive sacrificial ZnO template and their electrochromic property, Mater. Lett. 61 (2007) 2632-2637.

[46] P. Yuan, X. Yin, H. He, D. Yang, L. Wang, J. Zhu, Investigation on the delaminated-pillared structure of TiO_2-PILC synthesized by $TiCl_4$ hydrolysis method, Micropor. Mesopor. Mater. 93 (2006) 240-247.

[47] S. Yamanaka, T. Nishihara, M. Hattori, Y. Suzuki, Preparation and properties of titania pillared clay, Mater. Chem. Phys. 17 (1987) 87-101.

[48] S.G. Hur, T. Kim, S. Hwang, J. Yang, J.Choy, Heterostructured Nanohybrid of Zinc Oxide-Montmorillonite Clay, J. Phys. Chem. B 110 (2006) 1599-1604.

[49] K.O. Adebowale, I.E. Unuabonah, B.I. Olu-Owolabi, The effect of some operating variables on the adsorption of lead and cadmium ions on kaolinite clay, J. Hazard. Mater. B134 (2006) 130-139.

[50] F. Rozada, M. Otero, A. Moran, A. Garcıa, Adsorption of heavy metals onto sewage sludge-derived materials, Bioresour. Techn. 99 (2008) 6332-6338.

[51] M. Aguado, S. Cervera-March, J. Giménez, Continuous photocatalytic treatment of mercury(II) on titania powders. Kinetics and catalyst activity, Chem. Eng. Sci. 50 (1995) 1561-1569.

[52] N.H. Turner, Kinetics of chemisorption: an examination of the Elovich equation, J. Catal. 36 (1975) 262–265.

[53] Y. Ho, Review of second-order models for adsorption systems, J. Hazard. Mater. 136 (2006) 681-689.

[54] A. Gunay, E. Arslankaya, I. Tosun, Lead removal from aqueous solution by natural and pretreated clinoptilolite: Adsorption equilibrium and kinetics, J. Hazard. Mater. 146 (2007) 362–371.

[55] M. Alkan, M. Doğan, Y. Turhan, Q. Mirbaş, P. Turan, Adsorption kinetics and mechanism of maxilon blue 5G dye on sepiolite from aqueous solutions, Chem. Eng. J. 139 (2008) 213-223.

[56] E. Bulut, M. Özacar, I. Şengil, Adsorption of malachite green onto bentonite: Equilibrium and kinetic studies and process design, Micropor. Mesopor. Mater. 115(2008) 234-246.

[57] C.O. Illanes, N.A. Ochoa, J. Marchese, Kinetic sorption of Cr(VI) into solvent impregnated porous microspheres, Chem. Eng. J. 136 (2008) 92-98.

[58] S.H. Chien, W.R. Clayton, Application of Elovich equation to the kinetics of phosphate release and sorption in soils, Soil Sci. Soc. Am. J. 44 (1980) 265–268.

[59] Y.S. Ho, G. McKay, A comparison of chemisorption kinetic models applied to pollutant removal on various sorbents, Process Saf. Environ. Protect. 76B (1998) 332–340.

[60] R. Tseng, F. Wu, R. Juang, Liquid-phase adsorption of dyes and phenols using pinewood-based activated carbons, Carbon 41 (2003) 487-495.

[61] S. Anandan, M. Yoon, Photocatalytic activities of the nano-sized TiO_2-supported Y-zeolites, J. Photochem. Photobiol. C: Photochem. Rev. 4 (2003) 5–18.

[62] M. Aguado, S. Cervera-March, J. Giménez, Continuous photocatalytic treatment of mercury(II) on titania powders. Kinetics and catalyst activity, Chem. Eng. Sci. 50 (1995) 1561-1569.

[63] Y. Li, X. Li, J. Li, J. Yin, Photocatalytic degradation of methyl orange by TiO_2-coated activated carbon and kinetic study, Water Res. 40 (2006) 1119-1126.

[64] C.G. Silva, J.L. Faria, Photochemical and photocataytic degradation of an azo dye in aqueous solution by UV irradiation, J. Photochem. Photobiol. A: Chem. 155 (2003) 133–143.

[65] J. Herrmann, M. Gravelle-Rumeau-Mailleau, P. Gravelle, A microcalorimetric study of metal-support interaction in the Pt/TiO_2 system, J. Catal. 104 (1987) 136-146.

Table 1. Properties of the two materials synthesized.

Material	Specific surface area (m^2 g^{-1})	Pore volume (cm^3 g^{-1})	Avg. pore size (nm)
TiO_2 nanoparticles	210.1	0.213	0.82
TiO_2/montmorillonite	239.0	0.558	3.10

Table 2. Chemical compositions of the purified montmorillonite and TiO_2/montmorillonite, (wt%).

Material	SiO_2	Al_2O_3	TiO_2	CaO	MgO	Na_2O	Others
Purified montmorillonite	69.8	12.5	0.1	3.0	3.3	2.6	8.7
TiO_2/montmorillonite	55.5	9.1	22.0	0.5	1.9	0.3	10.7

Table 3. Langmuir parameters corresponding to the fitting of the experimental equilibrium data.

Materials	T (^{0}C)	Q^0 (mg g^{-1})	K_L (L mg^{-1})	r	R
TiO_2 nanoparticles	25	101.1	0.0056	0.641	0.99993
	35	98.1	0.0053	0.654	0.99901
	45	90.4	0.0051	0.662	0.99854
TiO_2/montmorillonite	25	123.8	0.0054	0.650	0.99531
	35	118.3	0.0044	0.694	0.99889
	45	116.5	0.0037	0.730	0.99995

Table 4. Parameters of Elovich equation.

Samples	T ^{0}C	R	φ	θ	α (mg g^{-1} min^{-1})	β ($\times 10^{-2}$) (g mg^{-1})
TiO_2 nanoparticles	25	0.9940	-0.359	1.976	54.4	2.79
	35	0.9906	-0.329	1.908	48.8	3.03
	45	0.9944	-0.288	1.803	41.8	3.47
TiO_2/montmorillonite	25	0.9935	-0.396	2.029	65.5	2.52
	35	0.9960	-0.373	1.995	58.6	2.68
	45	0.9886	-0.355	1.979	52.3	2.82

Table 5. Activation energies and pre-exponential factors.

Material	R	E_A (kJ mol^{-1})	k_o (min^{-1})
TiO_2 nanoparticles	0.9962	25.0	2.4×10^{-4}
TiO_2/montmorillonite	0.9998	22.6	9.3×10^{-5}

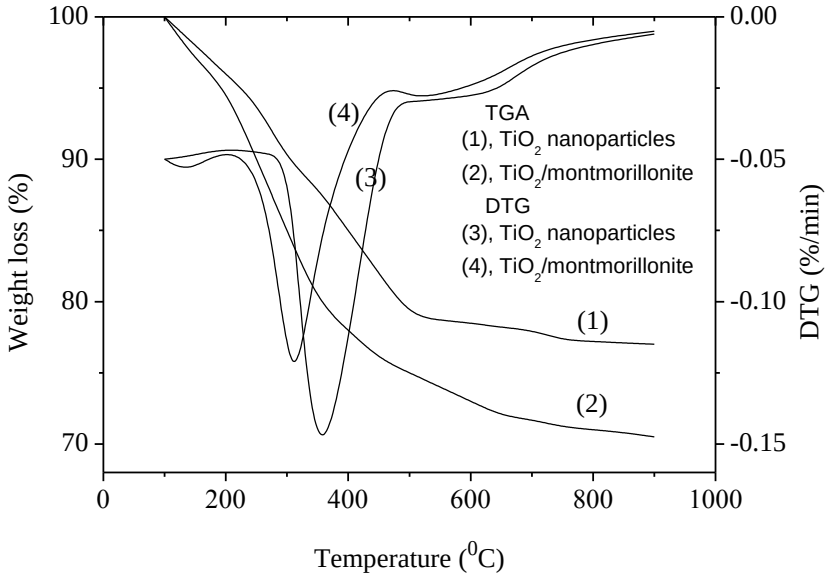

Fig. 1. TG-DTG curves of the two material precursors.

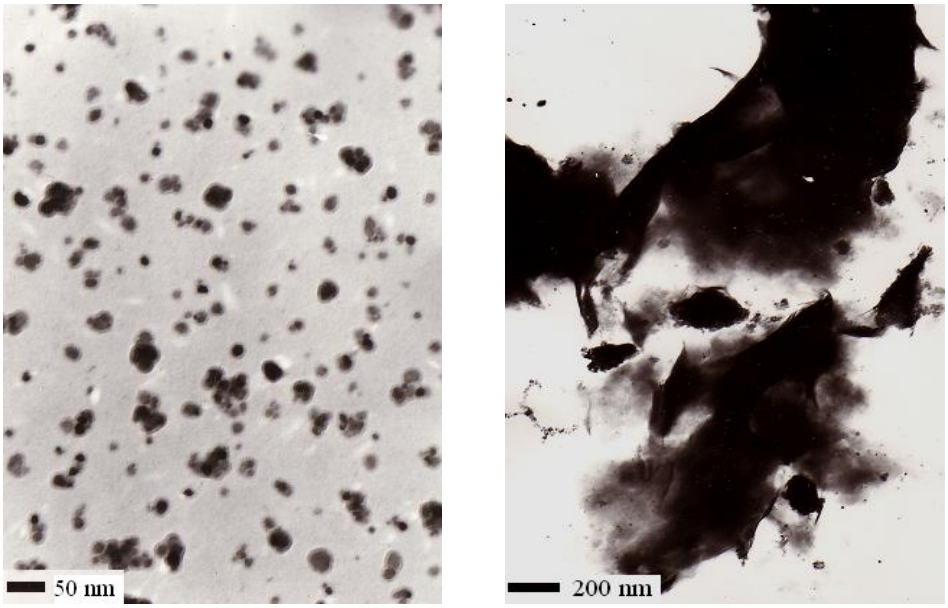

(a) (b)

Fig. 2. TEM images of (a) TiO_2 nanoparticles and (b) TiO_2/montmorillonite.

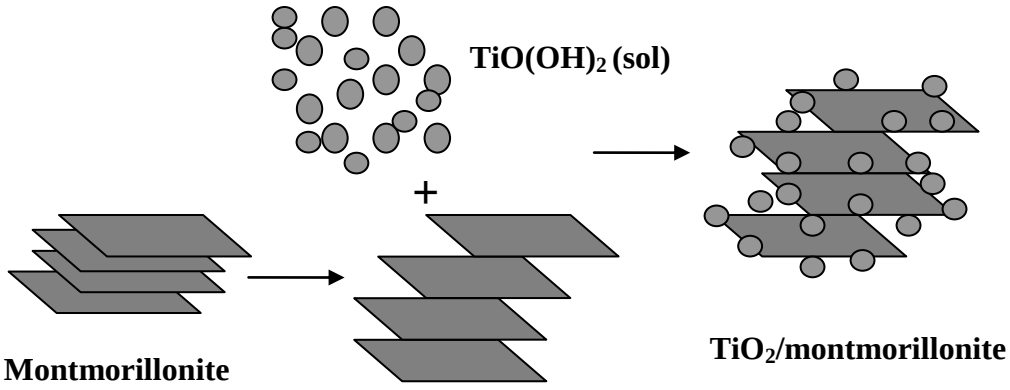

Fig. 3. Schematic diagram of the preparation method of TiO_2/montmorillonite.

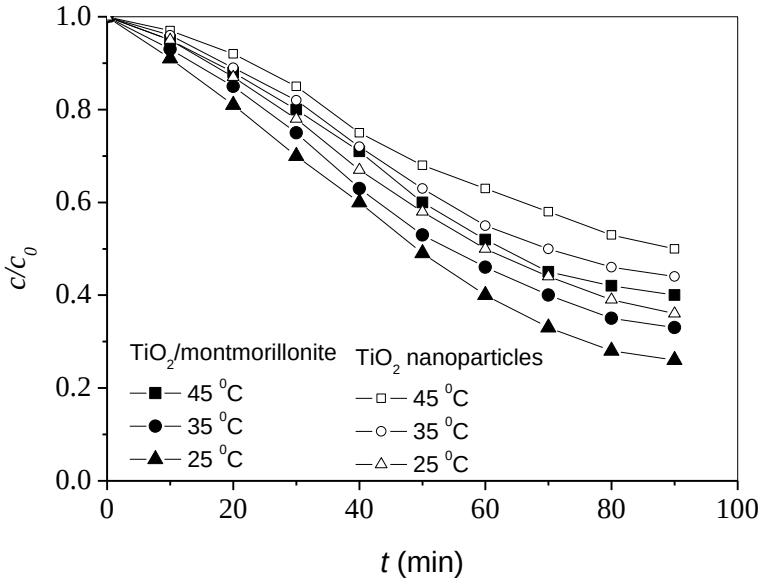

Fig. 4. Decreasing Hg(II) concentrations with time by adsorption at the different temperatures in aqueous solutions.

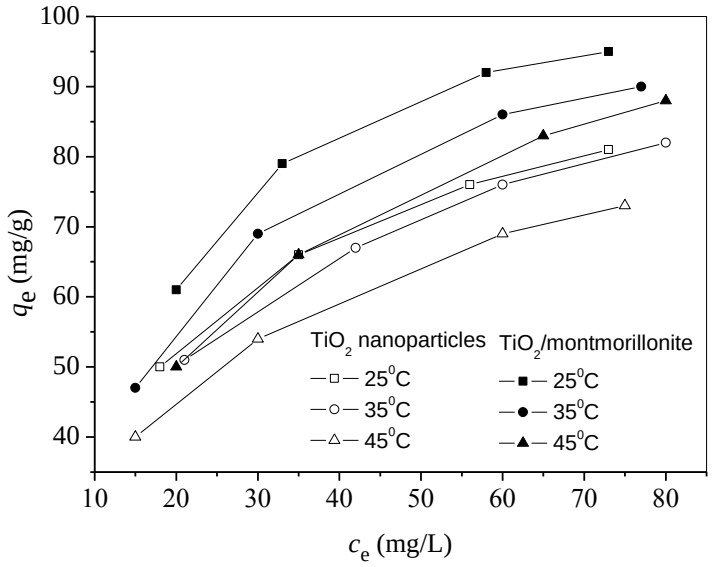

Fig. 5. Experimental equilibrium results of the adsorption of Hg(II).

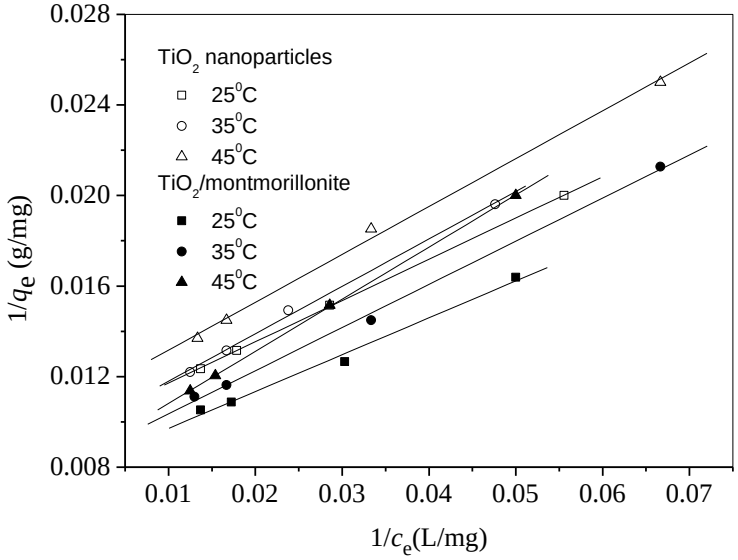

Fig. 6. Fitting results of Langmuir isotherm model.

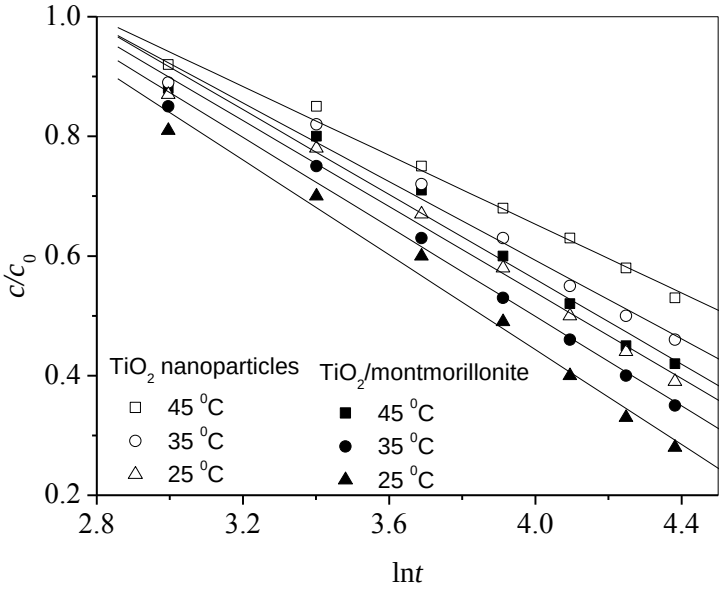

Fig. 7. Relationship of c/c_0 and $\ln t$ in the adsorption of Hg(II).

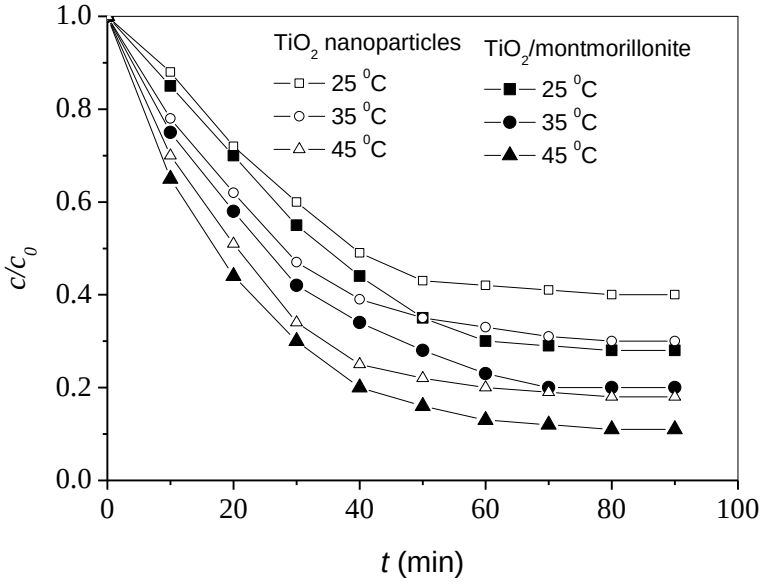

Fig. 8. Decreasing Hg(II) concentrations with time by photocatalytic reduction at the different temperatures in aqueous solutions.

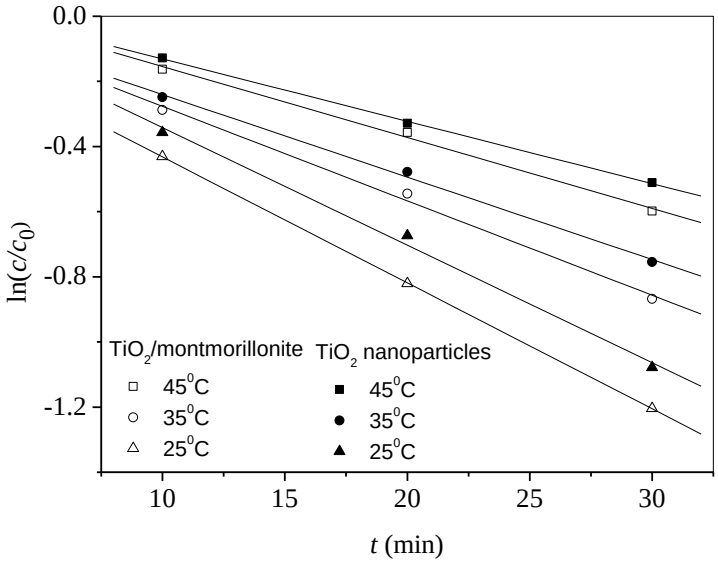

Fig. 9. Relationship between ln(c/c_0) and t at the different temperatures in the initial time of 30 min in photocatalytic reduction of Hg(II).